Few-layer hexagonal boron nitride as a shield of brittle materials for cryogenic s-SNOM exploration of phonon polaritons

Debo Hu,[1] Cheng Luo,[1] Lixing Kang,[2] Mengkun Liu,[3] Qing Dai[1,a)]

[1]CAS Key Laboratory of Nanophotonic Materials and Devices, CAS Key Laboratory of Standardization and Measurement for Nanotechnology, CAS Center for Excellence in Nanoscience, National Center for Nanoscience and Technology, Beijing 100190, China

[2]Suzhou Institute of Nano-Tech and Nano-Bionics, CAS, Suzhou, 215123, China

[3]Department of Physics, Stony Brook University, Stony Brook, NY 11794, USA

[a)]Authors to whom correspondence should be addressed: daiq@nanoctr.cn

Abstract

Surface phonon polaritons (SPhPs) in van der Waals (vdW) materials are of great interest in fundamental and applied research fields. Probing the characteristics of vdW SPhPs at cryogenic temperatures is an essential task for their implementation in low-temperature physics. However, the most commonly used characterization technique of vdW SPhPs under ambient conditions – scattering-type scanning near-field optical microscopy (s-SNOM) operating in tapping mode (intermittent-contact mode) – can prove especially problematic at low temperatures because the sample under test may become brittle and fragile. Therefore, high fracture toughness is desired for the samples under intermittent-contact s-SNOM scanning at low temperatures. In this work, by taking α-phase molybdenum trioxide (α-MoO_3) as a representative, we first confirm the surface deterioration induced by tip-sample interactions at low temperatures as a primary obstacle hindering the cryogenic nano-imaging of vdW SPhPs using a tapping mode s-SNOM. Then, we propose to use few-layer hexagonal boron nitride (*h*BN) as a mechanically tough yet optically passive cladding layer to enhance the surface stability of α-MoO_3. Finally, we demonstrate the validity of our surface reinforcement strategy by probing the previously unexplored temperature dependence of SPhPs within the third Reststrahlen band (RB_3) of α-MoO_3. Our method allows a sustained operation of tapping mode s-SNOM at cryogenic temperatures with negligible effect on the intrinsic properties of SPhPs.

Owning to the development of advanced characterization techniques like scattering-type scanning near-field optical microscopy (s-SNOM)[1-6] and the emergence of low-dimensional materials like van der Waals (vdW) crystals,[7-12] recent years have witnessed a renaissance of the research on surface phonon polaritons (SPhPs).[13-16] The hybrid photon-phonon nature of SPhPs[17] together with the intrinsic low-dimensional character of vdW materials[18-20] make the associated electromagnetic energy extremely confined in space,[21,22] and therefore vdW SPhPs is a topic of intense current interest in both fundamental and technical research fields related to strong light-matter interactions.[23,24] Promising applications of vdW SPhPs include assisting the multiphoton spontaneous emission,[25] mediating the near-field and ballistic heat transfer,[26-28] enhancing the dynamical vacuum effects,[29] and improving the sensitivity of vibrational spectroscopy[30,31]. Many of which involve cryogenic operating conditions.[28,32,33] However, although cryogenic s-SNOM (cryo-SNOM) has been commercially available for several years[34,35] and graphene plasmon polaritons have been routinely probed by a couple of homebuilt cryo-SNOM systems,[36-41] reports on the near-field characterization of vdW SPhPs at cryogenic temperatures are rare so far.[42] This stems from specific difficulties in performing cryogenic nano-imaging of vdW SPhPs.

In this work, by taking the biaxial α-phase molybdenum trioxide (α-MoO_3) as a representative, we first identify the surface deterioration of the microcrystal under investigation induced by tip-sample interactions at low temperatures as the main obstacle hindering the cryogenic nano-imaging of vdW SPhPs using a tapping mode s-SNOM. Then, we propose to use few-layer hexagonal boron nitride (*h*BN) as a mechanically tough yet optically passive cladding layer to enhance the surface stability of α-MoO_3. Finally, we demonstrate the validity of our surface reinforcement strategy by probing the previously unexplored temperature dependence of SPhPs in the third Reststrahlen band (RB_3) of α-MoO_3.

s-SNOM operating in tapping mode (intermittent-contact mode) is not always non-invasive,[43,44] because there exists a time-varying (frequency f~270 kHz) interaction force up to tens of nN (free amplitude A~100 nm, 80% setpoint, cantilever force constant k~42 N/m, quality factor of tip~1000) between the vibrating tip and the sample surface,[45-47] which is equivalent to a high-rate stress on the order of GPa[48] as a result of the tiny contact area and can potentially damage the surfaces of specific samples. This is especially the case at cryogenic temperatures, since many materials undergo ductile-brittle transition when cooled down[49-52] and become more sensitive to the high-rate impact of the tip apex as a result of the deteriorated fracture toughness.[53,54] Considering a previous first principle calculation has suggested the surface stability of α-MoO_3 is temperature dependent,[55] we chose α-MoO_3 as a model material for the

experimental study of tip-induced surface deterioration at low temperatures and the corresponding protection strategy. Our imaging results obtained by a homebuilt cryo-SNOM system schematically illustrated in Figure 1(a) (see Figure S1 of the Supplementary Material for details inside the vacuum chamber) indeed indicate a reduced surface stability of α-MoO_3 at low temperature (Note that in all the experiments we used Arrow™ NCPt probes with their cantilevers micro-engineered. These processed probes exhibit comparable quality factors under vacuum-cryogenic conditions to those in ambient environment thus are nicknamed q_{Minus}). A typical near-field optical image of bare α-MoO_3 microcrystals mechanically exfoliated onto SiO_2/Si substrates at 88 K is shown in Figure 1(b), which indicates the rapid surface deterioration of α-MoO_3 during cryo-SNOM scanning makes the imaging of SPhPs extremely difficult (Such a problem has not been encountered under vacuum and room-temperature imaging conditions). To find out what happened in the scanning process, we took a close look at the tip apex used in the experiment with the scanning electron microscope (SEM), and the image shown in Figure 1(c) indicates there is some flaky debris attaching to the tip apex. Therefore, we conjecture that a probable scenario for the imaging process of Figure 1(b) is: first, the surface of α-MoO_3 became less stable as a result of low-temperature embrittlement and fractured under the repeated impact of SNOM tip; then, some fragments of the broken surface adhered to the tip apex; finally, the deteriorated sample surface together with the contaminated tip-apex cause a significant decay of the near-field signal.

To solve the problem of surface deterioration and tip contamination in the cryo-SNOM imaging, one has to resort to an appropriate cladding material that, on the one hand, can improve the mechanical toughness of the sample, and, on the other hand, would not disturb the optical imaging. Considering *h*BN exhibits a high fracture toughness thus is expected to be resistant to the impact of the tapping tip[56] and its Reststrahlen bands are well-separated from those of α-MoO_3 (in the frequency range from 850 to 1200 cm^{-1}, the real parts of the in-plane and the out-of-plane dielectric constants of *h*BN are positive while the imaginary parts are relatively small as shown in Figure S2 of the Supplementary Material),[57,58] we chose it to verify the validity of our surface reinforcement strategy. As shown in Figure 1(d), we fabricated a α-MoO_3 sample partly cladded with a 5-nm-thick *h*BN flake using the standard dry transfer method[59] and put it into the trial of cryo-SNOM scanning at 88 K. Three rounds of scanning (along the [100] direction and cross the sample edge) have been conducted with the first two on the bare α-MoO_3 surface and the last one on the partly cladded sample surface. Without exception, all bare α-MoO_3 surface areas have been modified considerably by scanning, as seen from the comparison between the as-prepared and post-scanning sample optical miccrographs. Only the

*h*BN cladded site remained completely intact after scanning. Figure 1(e) shows the atomic force microscope (AFM) image corresponding to the third round scanning, the direct contrast between the broken bare α-MoO_3 surface and the intact *h*BN-protected surface is strong evidence for the effectiveness of our surface reinforcement method.

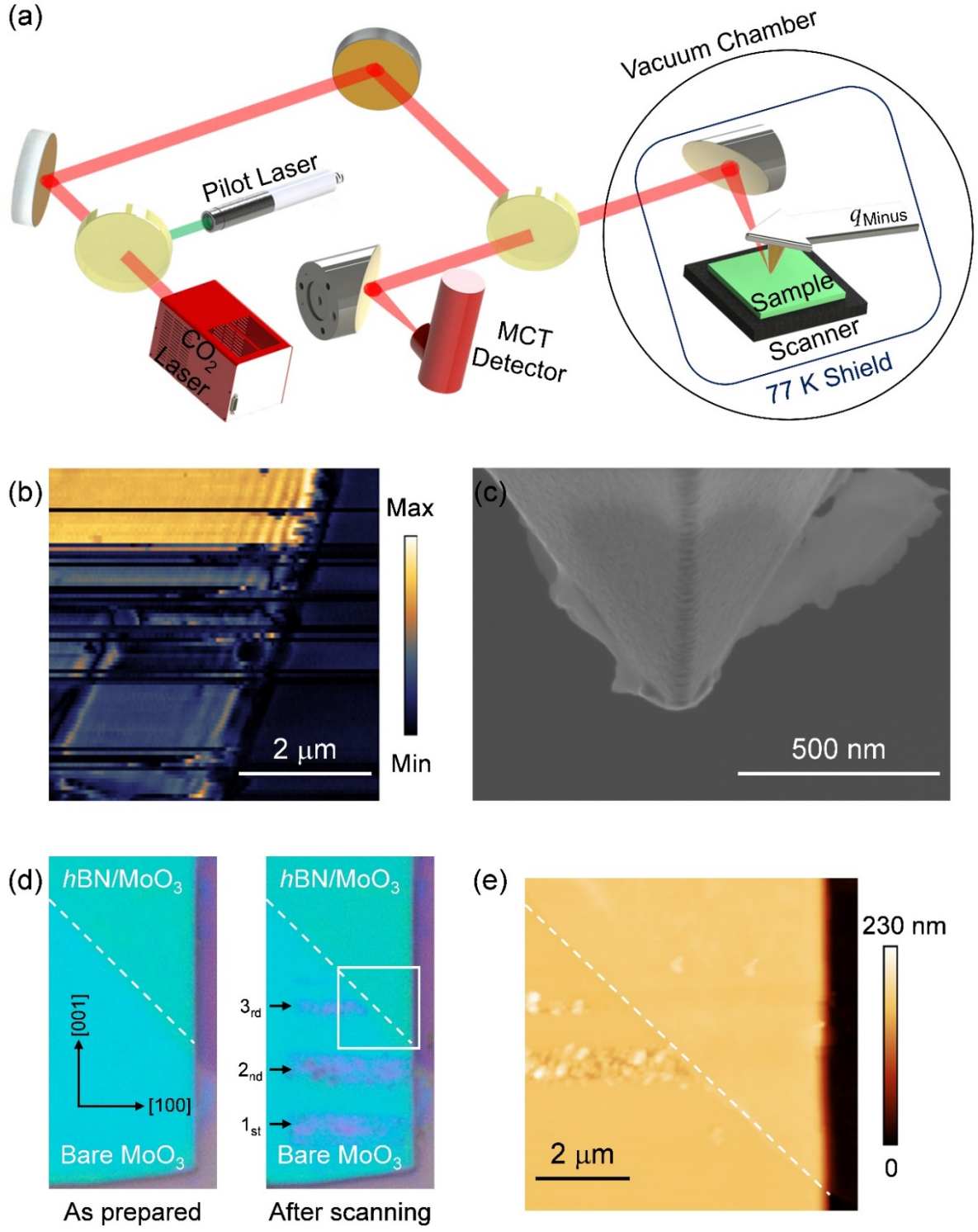

FIG. 1. (a) Schematics of the homebuilt cryo-SNOM system used in this work. (b) Near-field optical image indicating surface deterioration of bare α-MoO_3 induced by tip-sample interaction at 88 K. (c) SEM image of the SNOM tip apex used in (b). (d) Optical images of a

α-MoO_3 microcrystal partly cladded with a 5-nm-thick *h*BN flake before and after SNOM imaging at 88 K, the white dash lines indicate the *h*BN boundary, the black arrows in the right panel indicate the scanning area in each round of the experiment, and the box marks the imaging area in (e). (e) AFM image of the partly cladded α-MoO_3 sample marked in (d) with the box.

To evaluate the optical consequences of *h*BN cladding, using transfer-matrix method[60] and infrared dielectric parameters from references,[57,58,61] we calculated and compared the phonon-polariton behaviors of a SiO_2/130-nm-thick α-MoO_3/vacuum structure and a SiO_2/130-nm-thick α-MoO_3/*h*BN/vacuum model system within the RB_3 (960-1000 cm^{-1}) of α-MoO_3 with varying *h*BN thickness. Figure 2(a) and (b) show the dispersions of the fundamental phonon-polariton modes of α-MoO_3 propagating along the [100] ($M_{0,[100]}$) and [001] ($M_{0,[001]}$) crystalline directions, respectively. It can be seen that both $M_{0,[100]}$ and $M_{0,[001]}$ are type I hyperbolic phonon-polariton modes with negative phase velocity (negative real part of the effective indices of refraction N_{eff}) as a result of the negative out-of-plane dielectric constant of α-MoO_3 within RB_3,[8,58] and suffer high propagation losses below the frequency 970 cm^{-1} (large imaginary part of N_{eff}) resulting from the heavy damping of the nearby α-MoO_3 transverse optical phonon at 956.7 cm^{-1}.[58] Adding the *h*BN layer and increasing its thickness would generally compromise the field confinement factor (absolute value of the real part of N_{eff}) while lowering the propagation loss at the same time (decreasing imaginary part of N_{eff}). Specifically, in the case of $M_{0,[100]}$ the decrease of the propagation loss is more significant than that of the field confinement factor after *h*BN cladding, resulting in a net increase of the mode quality factor (Q=|Re(N_{eff})/Im(N_{eff})|) as shown in Figure 2(c) (the sharp dips are due to the transverse optical phonon of α-MoO_3 at 998.7 cm^{-1}); in the case of $M_{0,[001]}$ the decreases of the real and imaginary parts of N_{eff} are almost proportional, leading to a Q factor nearly independent of the *h*BN cladding as shown in Figure 2(d). Since the Q factors of both $M_{0,[100]}$ and $M_{0,[001]}$ have their maximum values in the frequency range from 980 cm^{-1} to 990 cm^{-1}, 985 cm^{-1} would be a preferred frequency in the following cryo-SNOM imaging experiments. To further assess the effect of *h*BN cladding on the excitation and detection of SPhPs at this selected frequency, we calculated the mode profiles (E_z components, with and without a 10-nm-thick *h*BN cladding layer) of $M_{0,[100]}$ and $M_{0.[001]}$, respectively, as shown in Figure 2(e) and (f). Considering the *h*BN cladding layer only slightly modifies the mode profiles and the near-field imaging-related E_z components still extend well above the sample surface, our surface reinforcement method of *h*BN cladding would not impede the cryo-SNOM imaging of α-MoO_3 SPhPs.

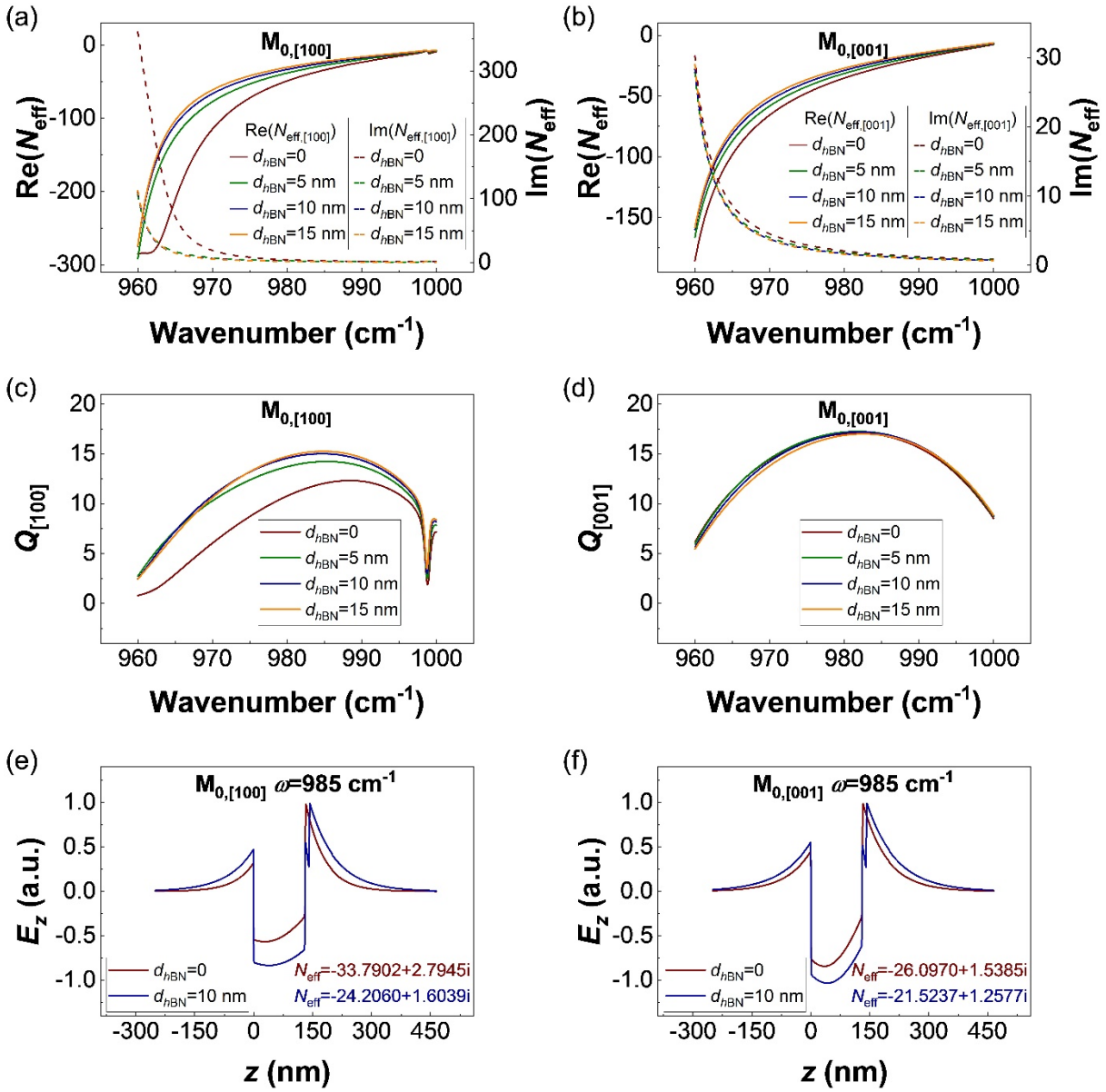

1 FIG. 2. (a) and (b) Calculated effective indices of refraction (N_{eff}) for the fundamental phonon-
2 polariton modes in the SiO_2/α-MoO_3/*h*BN/vacuum structure with a fixed α-MoO_3 thickness of
3 130 nm and varying *h*BN thickness, propagating along the [100] ($M_{0,[100]}$) and [001] ($M_{0.[001]}$)
4 crystalline directions of α-MoO_3 respectively. (c) and (d) *Q* factors of $M_{0,[100]}$ and $M_{0.[001]}$,
5 respectively. (e) and (f) Electric field profiles of $M_{0,[100]}$ and $M_{0.[001]}$ at 985 cm^{-1} with/without a
6 10-nm-thick *h*BN cladding layer, respectively.
7
8 Next, we proceeded to the experimental verification of the performance of *h*BN cladding
9 in the cryo-SNOM imaging of SPhPs. To this end, we fabricated a sample on SiO_2/Si substrate
10 by cladding a 130-nm-thick α-MoO_3 microcrystal with a 10-nm-thick *h*BN flake. Thanks to the
11 well-defined and mutually-orthogonal boundaries of this α-MoO_3 crystal, we can probe its
12 $M_{0,[100]}$ and $M_{0,[001]}$ modes simultaneously. In the imaging of $M_{0,[100]}$ ($M_{0,[001]}$) mode at 985 cm^{-}

[1] we scanned the sample along the [100] ([001]) direction and demodulated the near-field signal at the third-order harmonic of the tip-tapping frequency using a lock-in (O_3, lower-order signals recorded simultaneously usually exhibit inferior signal-to-noise ratio as shown in Figure S3 of the Supplementary Material). As shown in Figure 3(a), the sample surface survived the long-time high-rate impact of the SNOM tip and remained intact under the four different test temperatures. Interference fringes of both $M_{0,[100]}$ and $M_{0,[001]}$ caused by the vectorial superposition of the tip-launched and the edge-reflected SPhPs can be easily distinguished in all near-field optical images (O_3) at different temperatures. To enhance the visibility of the interference fringes in Figure 3(a) so as to facilitate the extraction of the propagation properties of both $M_{0,[100]}$ and $M_{0,[001]}$ at varying temperatures, we differentiated the images in Figure 3(a) along the [100] ($dO_3/dL_{[100]}$) and [001] ($dO_3/dL_{[001]}$) directions respectively and left the nearest fringes to the sample edges out before fitting the processed data with a damped sinusoidal waveform. Because the damped sinusoidal waveform and its derivative exhibit the same damping factor and spatial frequency, the differentiation process would not negatively influence the accuracy of data fitting.[62] We can see in Figure 3(b) that the processed experimental data fit very well with the damped sinusoidal waveform, and the extracted parameters from fitting for both $M_{0,[100]}$ and $M_{0,[001]}$ are illustrated in Figure 3(c) and (d). As predicted by the theoretical calculations in Figure 2, the $M_{0,[100]}$ mode indeed exhibits a more significant field confinement factor than that of $M_{0,[001]}$ while the $M_{0,[001]}$ mode holds a relatively higher Q factor, revealing the intrinsic in-plane optical anisotropy of α-MoO_3 across the entire temperature window explored. Thus far, the validity of our proposed surface reinforce method has been experimentally demonstrated, at least for α-MoO_3 on the most commonly used SiO_2/Si substrate. However, although the Q-temperature curves in Figure 3(d) (see Figure S4 of the Supplementary Material for results of a thicker sample) follow a similar trend with that of the type II hyperbolic phonon polaritons in bare α-MoO_3,[42] and the observed low-temperature Q factors are indeed larger than the theoretically predicted room-temperature ones, the wave-guiding properties of the type I hyperbolic phonon polaritons in *h*BN cladded α-MoO_3 do show slight non-monotonic temperature dependence within the investigated temperature range in our cryo-SNOM experiments. This non-monotonity might originate from the non-trivial strain imposed by the *h*BN cladding layer,[63] as evidenced by the different temperature dependence of the Raman spectrum of bare and cladded α-MoO_3 shown in Figure S5 of the Supplementary Material.

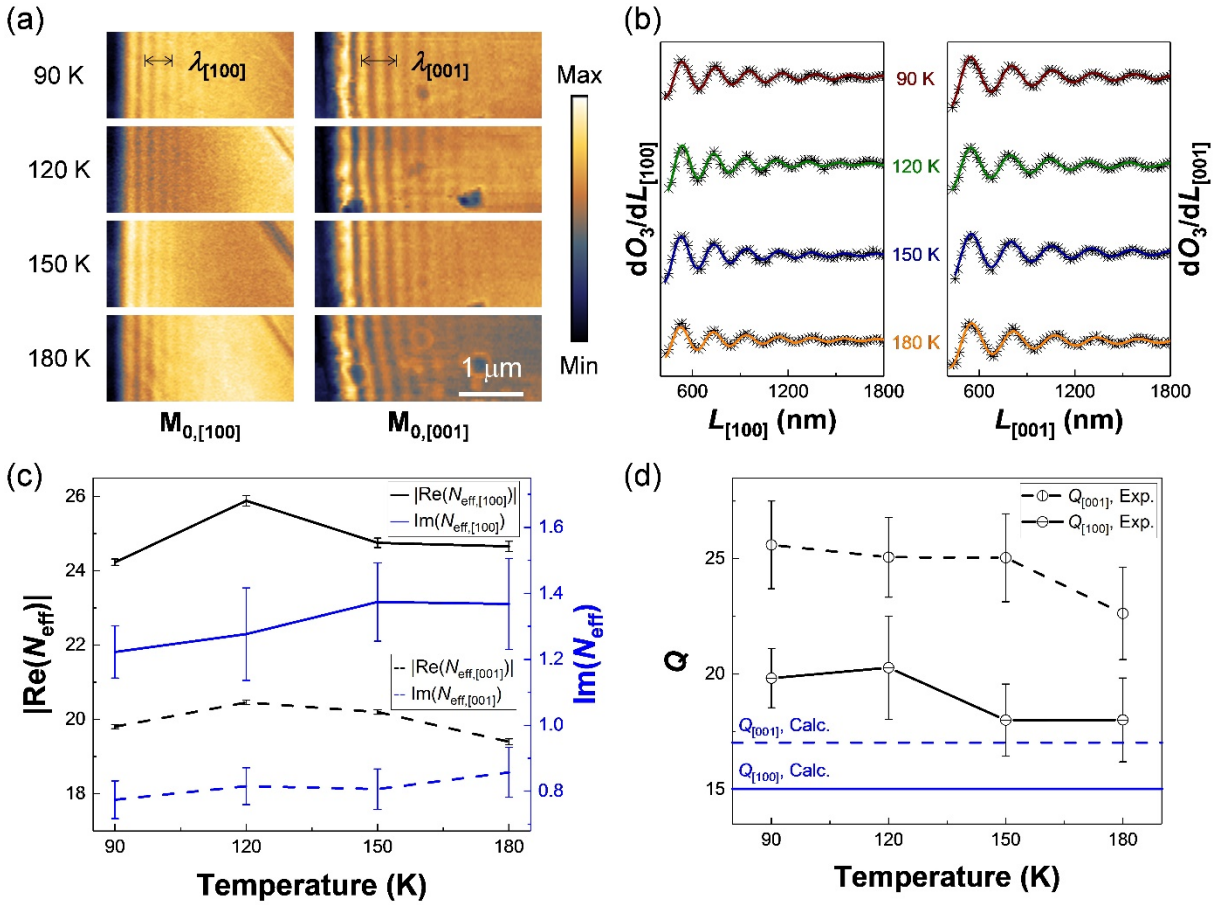

FIG. 3. (a) s-SNOM images of a 10-nm-thick *h*BN cladded 130-nm-thick α-MoO_3 microcrystal at cryogenic temperatures, along its [100] and [001] crystalline directions respectively. (b) Fitting the experimental data with a damped sinusoidal waveform. (c) Fitted effective indices of refraction (N_{eff}) at different temperatures. (d) Fitted *Q* factors at different temperatures, dash and solid horizontal lines indicate theoretically predicted room-temperature *Q* values for [001] and [100] directions respectively. Bars in (c) and (d) donate standard deviations.

To this day, cryo-SNOM remains one of a few diffraction-unlimited techniques which can probe the nanoscale electrodynamics of vdW crystals or other quantum materials at low temperatures.[64-67] Surface deterioration of samples under cryo-SNOM test induced by tip-sample interactions is an aspect not appreciated before. We first raise awareness of this problem, propose and verify an effective way of bypassing this obstacle in this work via *h*BN cladding. Using this method, we reveal the temperature dependence of the waveguiding properties of the type I hyperbolic phonon polaritons within RB_3 of α-MoO_3. Our method allows a sustained operation of tapping mode s-SNOM at cryogenic temperatures with negligible effect on the intrinsic properties of the sample, thus can be adopted as a standard method and used in the imaging of other polaritons like surface exciton polaritons[68-70], Cooper pair polaritons[71], and

surface magnon polaritons[72-74] at low temperatures. Besides, the s-SNOM imaging of brittle materials at ambient temperature can also benefit from this method.

Supplementary Material

A description of the cryo-SNOM assembly inside the vacuum chamber, an explanation about the applicable frequency range of the *h*BN protection layer, a comparison between the second- and third-harmonic demodulated images, the experimental results of a thicker α-MoO_3 sample, and the low-temperature Raman measurements results are included.

Q.D. acknowledges the support from the National Natural Science Foundation of China (Grant No. 51925203). D.H. acknowledges the support from the National Natural Science Foundation of China (Grant No. 52072083) and the Youth Innovation Promotion Association, CAS. Building of the cryo-SNOM used in this work is supported by the CAS Scientific Equipment Development Project. D.H. acknowledges Prof. S.P. Sun for the communications about MoO_3 surface stability, Prof. M.X. Liu and Prof. G.J. Zhang for the discussions on tip-sample interactions, and Dr. S.C. Sun for the help in low-temperature Raman measurements.

DATA AVAILABILITY

The data that support the findings of this study are available from the corresponding author upon reasonable request.

REFERENCES

[1]F. Keilmann, J. Microsc. **194**, 567 (1999).

[2]A. Huber, N. Ocelic, D. Kazantsev, and R. Hillenbrand, Appl. Phys. Lett. **87**, 81103 (2005).

[3]A. J. Huber, B. Deutsch, L. Novotny, and R. Hillenbrand, Appl. Phys. Lett. **92**, 203104 (2008).

[4]A. J. Huber, N. Ocelic and R. Hillenbrand, J. Microsc. **229**, 389 (2008).

[5]X. Chen, D. Hu, R. Mescall, G. You, D. N. Basov, Q. Dai, and M. Liu, Adv. Mater. **31**, 1804774 (2019).

[6]W. Ma, G. Hu, D. Hu, R. Chen, T. Sun, X. Zhang, Q. Dai, Y. Zeng, A. Alù, C. Qiu, and P. Li, Nature **596**, 362 (2021).

[7]S. Dai, Z. Fei, Q. Ma, A. S. Rodin, M. Wagner, A. S. McLeod, M. K. Liu, W. Gannett, W. Regan, K. Watanabe, T. Taniguchi, M. Thiemens, G. Dominguez, A. H. C. Neto, A. Zettl, F. Keilmann, P. Jarillo-Herrero, M. M. Fogler, and D. N. Basov, Science **343**, 1125 (2014).

[8]E. Yoxall, M. Schnell, A. Y. Nikitin, O. Txoperena, A. Woessner, M. B. Lundeberg, F. Casanova, L. E. Hueso, F. H. L. Koppens, and R. Hillenbrand, Nat. Photonics **9**, 674 (2015).

[9]P. Li, I. Dolado, F. J. Alfaro-Mozaz, F. Casanova, L. E. Hueso, S. Liu, J. H. Edgar, A. Y. Nikitin, S. Vélez, and R. Hillenbrand, Science **359**, 892 (2018).

[10]W. Ma, P. Alonso-González, S. Li, A. Y. Nikitin, J. Yuan, J. Martín-Sánchez, J. Taboada-Gutiérrez, I. Amenabar, P. Li, S. Vélez, C. Tollan, Z. Dai, Y. Zhang, S. Sriram, K. Kalantar-Zadeh, S. Lee, R. Hillenbrand, and Q. Bao, Nature **562**, 557 (2018).

[11]Z. Zheng, N. Xu, S. L. Oscurato, M. Tamagnone, F. Sun, Y. Jiang, Y. Ke, J. Chen, W. Huang, W. L. Wilson, A. Ambrosio, S. Deng, and H. Chen, Sci. Adv. **5**, v8690 (2019).

[12]J. Taboada-Gutiérrez, G. Álvarez-Pérez, J. Duan, W. Ma, K. Crowley, I. Prieto, A. Bylinkin, M. Autore, H. Volkova, K. Kimura, T. Kimura, M. H. Berger, S. Li, Q. Bao, X. P. A. Gao, I. Errea, A. Y. Nikitin, R. Hillenbrand, J. Martín-Sánchez, and P. Alonso-González, Nat. Mater. **19**, 964 (2020).

[13]J. D. Caldwell, L. Lindsay, V. Giannini, I. Vurgaftman, T. L. Reinecke, S. A. Maier, and O. J. Glembocki, Nanophotonics **4**, 44 (2015).

[14]D. N. Basov, M. M. Fogler and F. J. García De Abajo, Science **354**, g1992 (2016).

[15]T. Low, A. Chaves, J. D. Caldwell, A. Kumar, N. X. Fang, P. Avouris, T. F. Heinz, F. Guinea, L. Martin-Moreno, and F. Koppens, Nat. Mater. **16**, 182 (2017).

[16]J. D. Caldwell, I. Aharonovich, G. Cassabois, J. H. Edgar, B. Gil, and D. N. Basov, Nat. Rev. Mater. **4**, 552 (2019).

[17]D. N. Basov, A. Asenjo-Garcia, P. J. Schuck, X. Zhu, and A. Rubio, Nanophotonics **10**, 549 (2021).

[18]K. S. Novoselov, D. Jiang, F. Schedin, T. J. Booth, V. V. Khotkevich, S. V. Morozov, and A. K. Geim, Proc. Natl Acad. Sci. USA **102**, 10451 (2005).

[19]A. K. Geim and I. V. Grigorieva, Nature **499**, 419 (2013).

[20]K. S. Novoselov, A. Mishchenko, A. Carvalho, and A. H. Castro Neto, Science **353**, 461 (2016).

[21]S. Dai, W. Fang, N. Rivera, Y. Stehle, B. Jiang, J. Shen, R. Y. Tay, C. J. Ciccarino, Q. Ma, D. Rodan-Legrain, P. Jarillo-Herrero, E. H. T. Teo, M. M. Fogler, P. Narang, J. Kong, and D. N. Basov, Adv. Mater. **31**, 1806603 (2019).

[22]N. Li, X. Guo, X. Yang, R. Qi, T. Qiao, Y. Li, R. Shi, Y. Li, K. Liu, Z. Xu, L. Liu, F. J. García De Abajo, Q. Dai, E. Wang, and P. Gao, Nat. Mater. **20**, 43 (2021).

[23]N. Rivera, T. Christensen and P. Narang, Nano Lett. **19**, 2653 (2019).

[24]N. Rivera and I. Kaminer, Nat. Rev. Phys. **2**, 538 (2020).

[25]N. Rivera, G. Rosolen, J. D. Joannopoulos, I. Kaminer, and M. Soljačić, Proc. Natl Acad. Sci. USA (2017).

[26]B. Song, A. Fiorino, E. Meyhofer, and P. Reddy, AIP Adv. **5**, 53503 (2015).

[27]B. Zhao, B. Guizal, Z. M. Zhang, S. Fan, and M. Antezza, Phys. Rev. B **95**, 245437 (2017).

[28]S. Huberman, R. A. Duncan, K. Chen, B. Song, V. Chiloyan, Z. Ding, A. A. Maznev, G. Chen, and K. A.

Nelson, Science **364**, 375 (2019).

[29]J. Sloan, N. Rivera, J. D. Joannopoulos, and M. Soljačić, Phys. Rev. Lett. **127**, 53603 (2021).

[30]M. Autore, P. Li, I. Dolado, F. J. Alfaro-Mozaz, R. Esteban, A. Atxabal, F. Casanova, L. E. Hueso, P. Alonso-González, J. Aizpurua, A. Y. Nikitin, S. Vélez, and R. Hillenbrand, Light. Sci. Appl. **7**, 17172 (2018).

[31]A. Bylinkin, M. Schnell, M. Autore, F. Calavalle, P. Li, J. Taboada-Gutièrrez, S. Liu, J. H. Edgar, F. Casanova, L. E. Hueso, P. Alonso-Gonzalez, A. Y. Nikitin, and R. Hillenbrand, Nat. Photonics **15**, 197 (2020).

[32]G. Plunien, R. Schützhold and G. Soff, Phys. Rev. Lett. **84**, 1882 (2000).

[33]C. M. Wilson, G. Johansson, A. Pourkabirian, M. Simoen, J. R. Johansson, T. Duty, F. Nori, and P. Delsing, Nature **479**, 376 (2011).

[34]T. Gokus, A. Huber and M. Eisele, presented at the 2018 Conference on Lasers and Electro-Optics (CLEO), San Jose, California United States, 2018.

[35]W. Luo, M. Boselli, J. Poumirol, I. Ardizzone, J. Teyssier, D. van der Marel, S. Gariglio, J. Triscone, and A. B. Kuzmenko, Nat. Commun. **10**, 2774 (2019).

[36]H. U. Yang, E. Hebestreit, E. E. Josberger, and M. B. Raschke, Rev. Sci. Instrum. **84**, 23701 (2013).

[37]G. X. Ni, A. S. McLeod, Z. Sun, L. Wang, L. Xiong, K. W. Post, S. S. Sunku, B. Y. Jiang, J. Hone, C. R. Dean, M. M. Fogler, and D. N. Basov, Nature **557**, 530 (2018).

[38]D. J. Rizzo, B. S. Jessen, Z. Sun, F. L. Ruta, J. Zhang, J. Yan, L. Xian, A. S. McLeod, M. E. Berkowitz, K. Watanabe, T. Taniguchi, S. E. Nagler, D. G. Mandrus, A. Rubio, M. M. Fogler, A. J. Millis, J. C. Hone, C. R. Dean, and D. N. Basov, Nano Lett. **20**, 8438 (2020).

[39]W. Zhao, H. Li, X. Xiao, Y. Jiang, K. Watanabe, T. Taniguchi, A. Zettl, and F. Wang, Nano Lett. **21**, 3106 (2021).

[40]Y. Dong, L. Xiong, I. Y. Phinney, Z. Sun, R. Jing, A. S. McLeod, S. Zhang, S. Liu, F. L. Ruta, H. Gao, Z. Dong, R. Pan, J. H. Edgar, P. Jarillo-Herrero, L. S. Levitov, A. J. Millis, M. M. Fogler, D. A. Bandurin, and D. N. Basov, Nature **594**, 513 (2021).

[41]W. Zhao, S. Zhao, H. Li, S. Wang, S. Wang, M. I. B. Utama, S. Kahn, Y. Jiang, X. Xiao, S. Yoo, K. Watanabe, T. Taniguchi, A. Zettl, and F. Wang, Nature **594**, 517 (2021).

[42]G. Ni, A. S. McLeod, Z. Sun, J. R. Matson, C. F. B. Lo, D. A. Rhodes, F. L. Ruta, S. L. Moore, R. A. Vitalone, R. Cusco, L. Artus, L. Xiong, C. R. Dean, J. C. Hone, A. J. Millis, M. M. Fogler, J. H. Edgar, J. D. Caldwell, and D. N. Basov, Nano Lett. **21**, 5767 (2021).

[43]M. Yu, T. Kowalewski and R. S. Ruoff, Phys. Rev. Lett. **85**, 1456 (2000).

[44]K. Bian, C. Gerber, A. J. Heinrich, D. J. Müller, S. Scheuring, and Y. Jiang, Nat. Rev. Methods Primers **1**, 36

(2021).

[45]R. García and A. San Paulo, Phys. Rev. B **60**, 4961 (1999).

[46]S. C. Fain, K. A. Barry, M. G. Bush, B. Pittenger, and R. N. Louie, Appl. Phys. Lett. **76**, 930 (2000).

[47]S. Hu and A. Raman, Appl. Phys. Lett. **91**, 123106 (2007).

[48]O. P. Behrend, F. Oulevey, D. Gourdon, E. Dupas, A. J. Kulik, G. Gremaud, and N. A. Burnham, Appl. Phys. A **66**, S219 (1998).

[49]A. W. Magnusson and W. M. Baldwin, J. Mech. Phys. Solids **5**, 172 (1957).

[50]D. A. Wigley, *Mechanical Properties of Materials at Low Temperatures*. (Springer, Boston, 1971).

[51]A. Lupinacci, J. Kacher, A. A. Shapiro, P. Hosemann, and A. M. Minor, J. Mater. Res. **36**, 1751 (2021).

[52]H. Kim and S. Roberts, J. Am. Ceram. Soc. **77**, 3099 (1994).

[53]K. S. Chan, Metall. Mater. Trans. A **34**, 2315 (2003).

[54]E. Frutos, J. L. González-Carrasco and T. Polcar, J. Eur. Ceram. Soc. **36**, 3235 (2016).

[55]S. P. Sun, J. L. Zhu, S. Gu, X. P. Li, W. N. Lei, Y. Jiang, D. Q. Yi, and G. H. Chen, Appl. Surf. Sci. **467-468**, 753 (2019).

[56]Y. Yang, Z. Song, G. Lu, Q. Zhang, B. Zhang, B. Ni, C. Wang, X. Li, L. Gu, X. Xie, H. Gao, and J. Lou, Nature **594**, 57 (2021).

[57]C. H. Perry, G. Rupprecht and R. Geick, Phys. Rev. **146**, 543 (1966).

[58]G. Álvarez-Pérez, T. G. Folland, I. Errea, J. Taboada-Gutiérrez, J. Duan, J. Martín-Sánchez, A. I. F. Tresguerres-Mata, J. R. Matson, A. Bylinkin, M. He, W. Ma, Q. Bao, J. I. Martín, J. D. Caldwell, A. Y. Nikitin, and P. Alonso-González, Adv. Mater. **32**, 1908176 (2020).

[59]L. Wang, I. Meric, P. Y. Huang, Q. Gao, Y. Gao, H. Tran, T. Taniguchi, K. Watanabe, L. M. Campos, D. A. Muller, J. Guo, P. Kim, J. Hone, K. L. Shepard, and C. R. Dean, Science **342**, 614 (2013).

[60]N. C. Passler and A. Paarmann, J. Opt. Soc. Am. B **34**, 2128 (2017).

[61]J. Kischkat, S. Peters, B. Gruska, M. Semtsiv, M. Chashnikova, M. Klinkmüller, O. Fedosenko, S. Machulik, A. Aleksandrova, G. Monastyrskyi, Y. Flores, and W. Ted Masselink, Appl. Opt. **51**, 6789 (2012).

[62]G. X. Ni, L. Wang, M. D. Goldflam, M. Wagner, Z. Fei, A. S. McLeod, M. K. Liu, F. Keilmann, B. Özyilmaz, A. H. C. Neto, J. Hone, M. M. Fogler, and D. N. Basov, Nat. Photonics **10**, 244 (2016).

[63]X. Sun, J. Shi, M. A. Washington, and T. Lu, Appl. Phys. Lett. **111**, 151603 (2017).

[64]H. F. Hess, E. Betzig, T. D. Harris, L. N. Pfeiffer, and K. W. West, Science **264**, 1740 (1994).

[65]J. M. Atkin, S. Berweger, A. C. Jones, and M. B. Raschke, Adv. Phys. **61**, 745 (2012).

[66]M. Liu, A. J. Sternbach and D. N. Basov, Rep. Prog. Phys. **80**, 14501 (2017).

[67]A. Tomadin, A. Principi, J. C. W. Song, L. S. Levitov, and M. Polini, Phys. Rev. Lett. **115**, 87401 (2015).

[68]J. Lagois and B. Fischer, Phys. Rev. Lett. **36**, 680 (1976).

[69]F. DeMartini, M. Colocci, S. E. Kohn, and Y. R. Shen, Phys. Rev. Lett. **38**, 1223 (1977).

[70]L. Schultheis and J. Lagois, Solid State Commun. **44**, 1557 (1982).

[71]M. E. Berkowitz, B. S. Y. Kim, G. Ni, A. S. McLeod, C. F. B. Lo, Z. Sun, G. Gu, K. Watanabe, T. Taniguchi, A. J. Millis, J. C. Hone, M. M. Fogler, R. D. Averitt, and D. N. Basov, Nano Lett. **21**, 308 (2021).

[72]R. Macêdo and R. E. Camley, Phys. Rev. B **99**, 14437 (2019).

[73]J. Sloan, N. Rivera, J. D. Joannopoulos, I. Kaminer, and M. Soljačić, Phys. Rev. B **100**, 235453 (2019).

[74]P. Sivarajah, A. Steinbacher, B. Dastrup, J. Lu, M. Xiang, W. Ren, S. Kamba, S. Cao, and K. A. Nelson, J. Appl. Phys. **125**, 213103 (2019).

Supplementary Material

for

Few-layer hexagonal boron nitride as a shield of brittle materials for cryogenic s-SNOM exploration of phonon polaritons

Debo Hu,[1] Cheng Luo,[1] Lixing Kang,[2] Mengkun Liu,[3] Qing Dai[1,a)]

[1]CAS Key Laboratory of Nanophotonic Materials and Devices, CAS Key Laboratory of Standardization and Measurement for Nanotechnology, CAS Center for Excellence in Nanoscience, National Center for Nanoscience and Technology, Beijing 100190, China

[2]Suzhou Institute of Nano-Tech and Nano-Bionics, CAS, Suzhou, 215123, China

[3]Department of Physics, Stony Brook University, Stony Brook, NY 11794, USA

[a)]Authors to whom correspondence should be addressed: daiq@nanoctr.cn

1. cryo-SNOM assembly inside the vacuum chamber

An annotated view of our cryo-SNOM inside the vacuum chamber is shown in Figure S1.

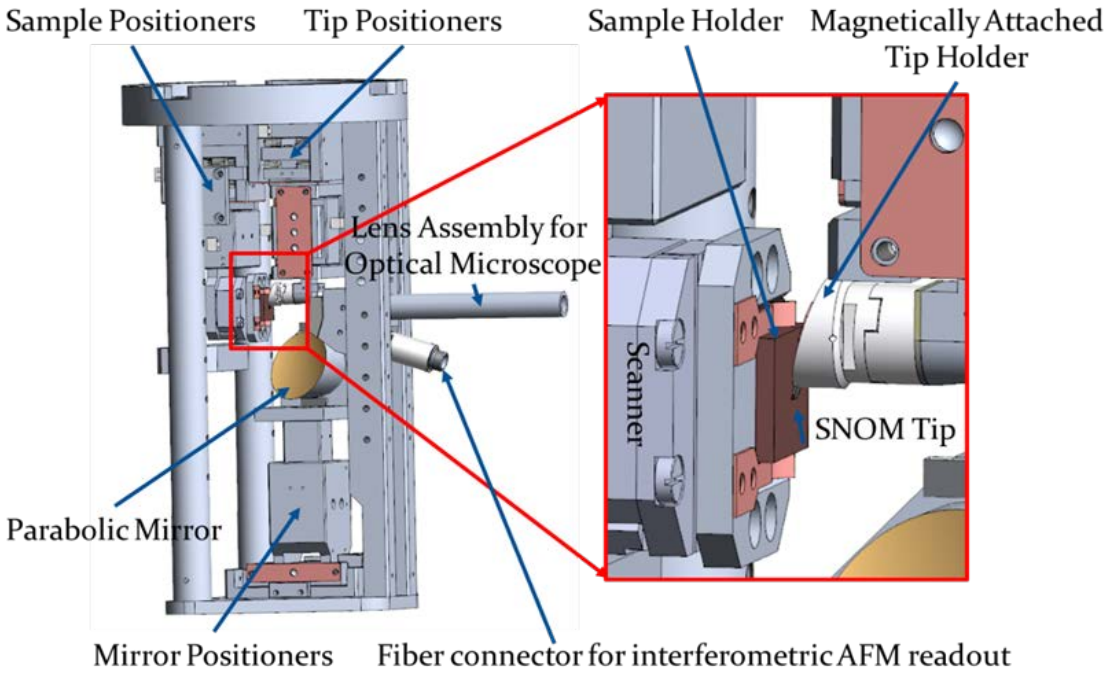

FIG. S1. 3D view of the cryo-SNOM assembly inside the vacuum chamber.

2. Applicable frequency range of the *h*BN protection layer

As shown in Figure S2, the real parts of the in-plane and the out-of-plane dielectric constants of *h*BN are both positive in the frequency range from 850 to 1350 cm^{-1}, and the imaginary parts are both less than one in the frequency range from 800 to 1200 cm^{-1}. Therefore, to avoid mode coupling and additional loss induced by the *h*BN protection layer, it is appropriate to limit the *h*BN cladding method to the frequency range from 850 to 1200 cm^{-1}.

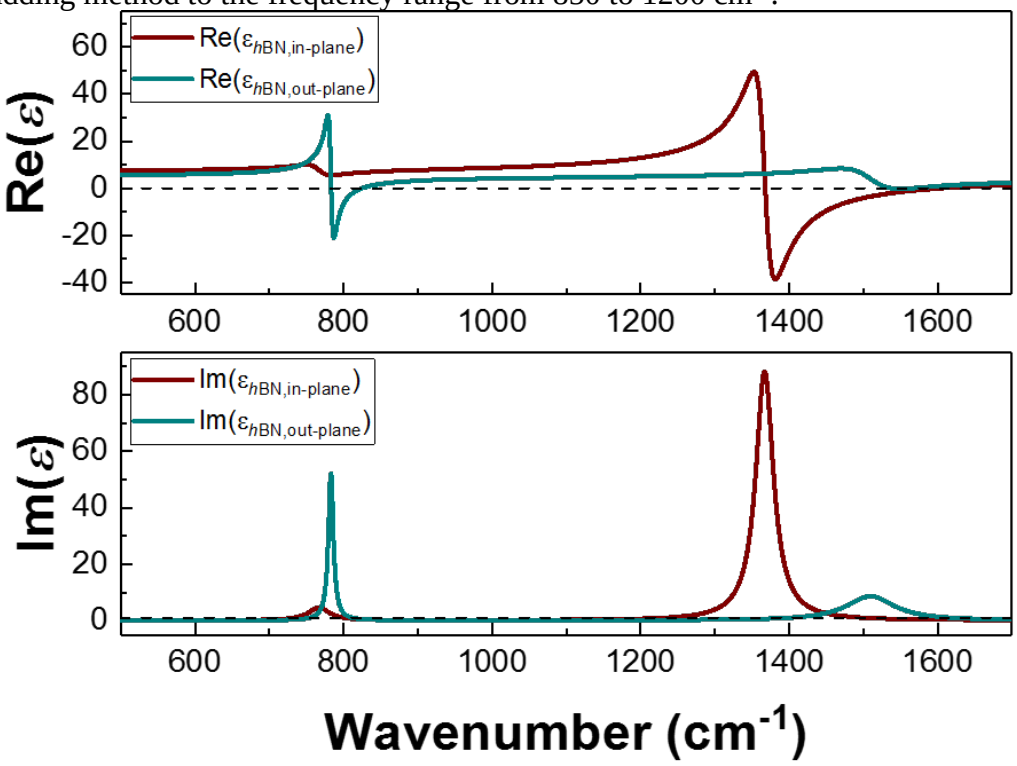

FIG. S2. Dielectric constants of *h*BN calculated based on the parameters from [Phys Rev 1966, 146, 543]. The horizontal dash lines in the upper and lower panels indicate the values zero and one, respectively.

3. Images of different demodulation order

The second- and third-harmonic demodulated cryo-SNOM images of the *h*BN cladded α-MoO_3 obtained at 90 K are shown in Figure S3. Compared with the third-harmonic demodulated image (O_3), the second-harmonic demodulated one (O_2) exhibits larger absolute signal magnitude but suffers from more background interference (a general rule of lock-in based demodulation techniques).

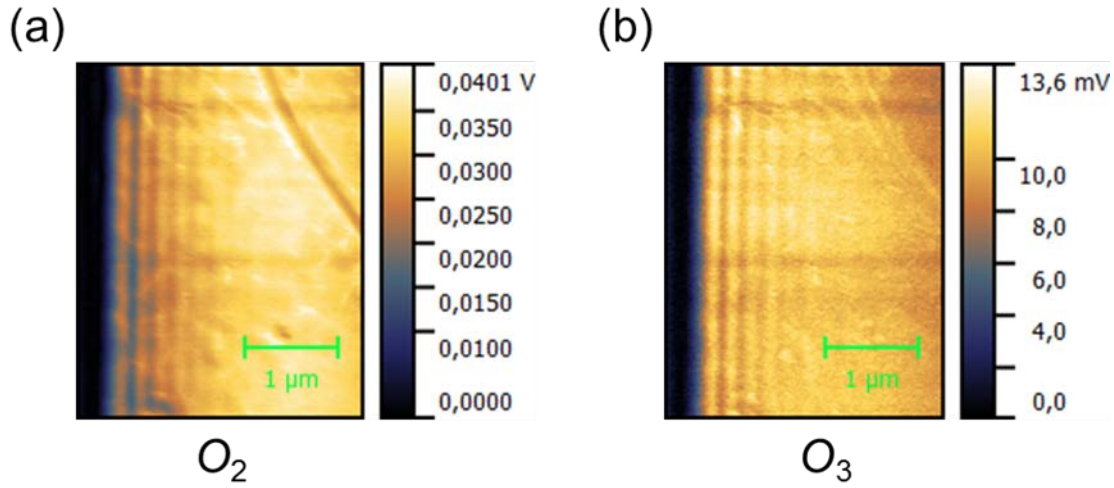

FIG. S3. (a) The second-harmonic demodulated cryo-SNOM image of *h*BN cladded α-MoO_3 obtained at 90 K. (b) The third-harmonic demodulated image.

4. Experimental results of a thicker MoO_3 sample

The Experimental results of a 155-nm-thick MoO_3 sample cladded with a 5-nm-thick *h*BN layer along the [100] direction are shown in Figure S4. As expected from theoretical calculations, the *Q* factors of this thicker MoO_3 are smaller than those of the thinner sample shown in Figure 3(d) in the maintext. But still, they are larger than the theoretically predicted one at room temperature.

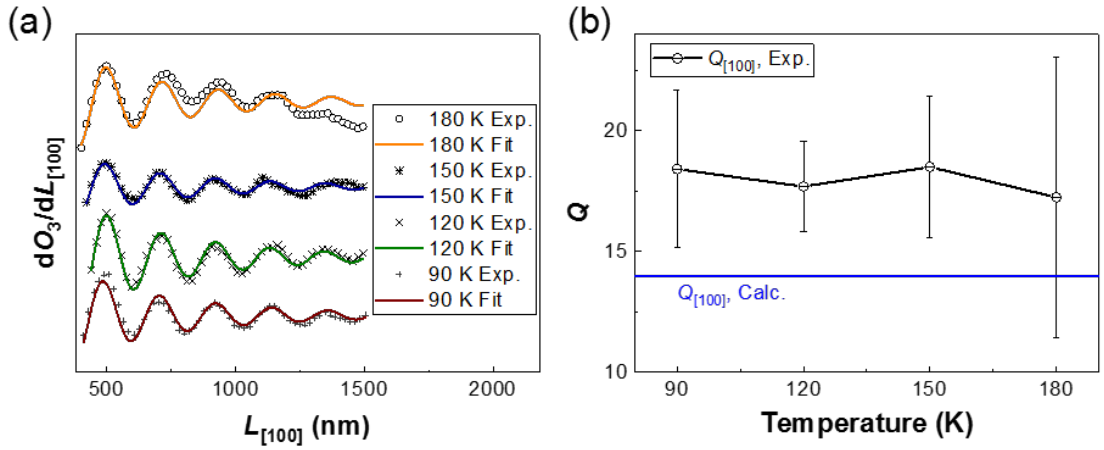

FIG. S4. (a) Experimental data points and fitted curves for the $M_{0,[100]}$ mode in a 155-nm-thick MoO_3 sample cladded with a 5-nm-thick *h*BN layer. (b) Fitted *Q* factors at low temperatures and the theoretically predicted *Q* factor at room temperature. Bars in (b) donate standard deviations.

5. Raman spectrum of bare and cladded MoO_3

Raman spectroscopy was used to evaluate whether the *h*BN cladding layer would impose a stress on MoO_3. As shown in Figure S5(a), the frequency shifts of the MoO_3 Raman mode near 820 cm^{-1} with the varying temperature seem to be suppressed by the *h*BN cladding layer. While the linewidths (full width at half maxima, FWHM) in the cladded case follow a similar trend with the varying temperature to that in the case of bare MoO_3 in Figure S5(b), they exhibit relatively smaller values. These differences between the Raman spectrum of the bare and the cladded MoO_3 suggest that non-trivial strain could be generated in the *h*BN/MoO_3 heterostructure and may play a role in causing the non-monotonic behaviours of the MoO_3 SPhPs observed in our cryo-SNOM experiments.

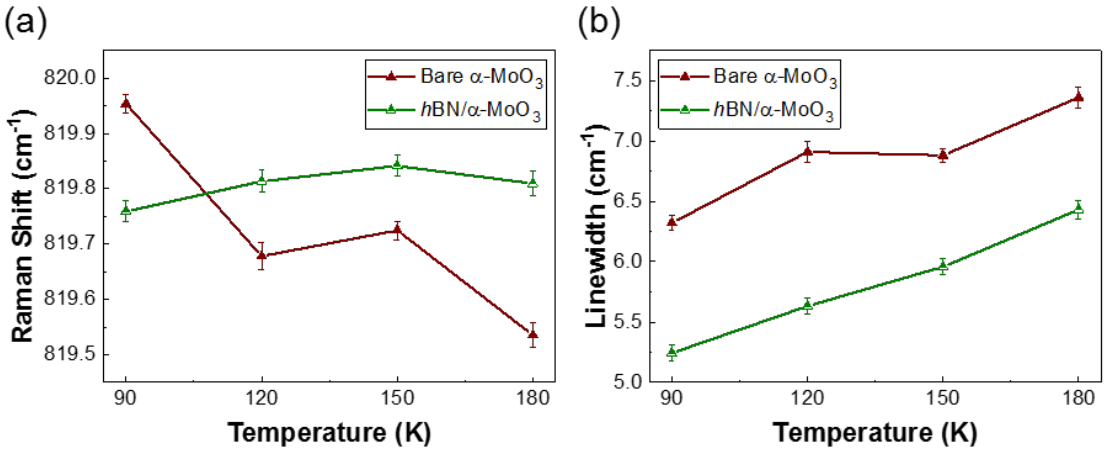

FIG. S5. (a) Temperature-dependent frequencies of the MoO_3 Raman mode near 820 cm^{-1}. (b) Temperature-dependent peak widths of the MoO_3 Raman mode near 820 cm^{-1}. Bars donate standard deviations.